ADVANCED ENERGY MATERIALS

Supporting Information

for *Adv. Energy Mater.,* DOI: 10.1002/aenm.201402276

Sputtered NiO_x Films for Stabilization of p^+n-InP Photoanodes for Solar-Driven Water Oxidation

*Ke Sun, Yanjin Kuang, Erik Verlage, Bruce S. Brunschwig, Charles W. Tu, and Nathan S. Lewis**

Supporting Information for:

Sputtered NiO_x Films for Stabilization of p^+n-InP Photoanodes for Solar-Driven Water Oxidation

Ke Sun[1,2], Yanjin Kuang[3], Erik A. Verlage[2,4], Bruce S. Brunschwig[2,5], Charles W. Tu[6], Nathan S. Lewis[1,2,5,7*]

Author Affiliations:

[1]Division of Chemistry and Chemical Engineering, California Institute of Technology, Pasadena, CA 91125, USA

[2]Joint Center for Artificial Photosynthesis, California Institute of Technology, Pasadena, CA 91125, USA

[3]Department of Physics, University of California, San Diego, La Jolla, CA 92093, USA

[4]Material Science, California Institute of Technology, Pasadena, CA 91125, USA

[5]Beckman Institute and Molecular Materials Research Center, California Institute of Technology, Pasadena, CA 91125, USA

[6]Department of Electrical and Computer Engineering, University of California, San Diego, La Jolla, CA 92093, USA

[7]Kavli Nanoscience Institute, California Institute of Technology, Pasadena, CA 91125, USA

Experimental:

Chemicals:

Except where otherwise noted, all materials were used as received, including potassium hydroxide pellets (KOH, Macron Chemicals, ACS 88%), boric acid (H_3BO_3, Sigma-Aldrich, BioReagent ≥99.5%), potassium ferrocyanide trihydrate ($K_4Fe(CN)_6 \cdot 3H_2O$, Acros, >99%), potassium ferricyanide ($K_3Fe(CN)_6$, Fisher Chemicals, certified ACS 99.4%), potassium chloride (KCl, Macron Chemicals, Granular ACS 99.6%), Br_2 (Sigma Aldrich, 99.999%), and CH_3OH (EMD Millipore, >99.9%). Water with a resistivity of 18.2 MΩ·cm was obtained from a Millipore deionized water system. Single-side polished, Sn-doped (N_d = 4.22-5.83×10^{17} cm^{-3}), (100)-oriented, n-type InP wafers were obtained from AXT Inc. Nominally undoped (N_d = 10^{15} cm^{-3}), (100)-oriented, n-type single-side-polished InP wafers were obtained from MTI Inc. Zn-doped (N_a = 3×10^{18} cm^{-3}), (100)-oriented, p-type single-side-polished InP wafers were obtained from MTI Inc.

Growth of the p^+n-InP junction:

All samples were grown on InP (001) epi-ready substrates in a Varian Gen-II Molecular-Beam Epitaxy (MBE) system that had been modified to thermally crack gas-phase PH_3 to P_2 and H_2. Elemental In and Be were used as group-III and p-type sources, respectively. At ~410 °C, the native oxide on the substrate surface was fully desorbed under the P_2 overpressure, as confirmed by streaky 2×4 surface reconstruction patterns observed using reflection high-energy electron diffraction (RHEED). The highly doped p^+-InP layer growth was triggered when the In shutter was opened and the InP film growth rate was set at 1 μm h^{-1} (i.e., 1 monolayer s^{-1}), as calibrated by the RHEED oscillations. The PH_3 flow rate was set at 6 sccm throughout the growth. The doping for these two samples was ~5×10^{18} cm^{-3}, as calibrated by Hall measurements on InP test film samples grown on semi-insulating InP substrates. A p^+-layer with a thickness of 100 nm was

grown on undoped crystalline n-InP. The growth was stopped when the targeted thickness was reached. After the growth, the sample was cooled to ~280 °C before flow of the PH_3 protection gas was stopped.

Hall measurement:

The mobile carrier concentration of the MBE-grown p^+-InP emitter layer (200 nm) was measured using the Van der Pauw method on a semi-insulating InP Fe-doped, (100) oriented wafer (AXT Inc). The Hall measurement was performed on 0.5×0.5 cm^2 square samples. The In contacts were applied on the four corners of the samples. A (0.7 T, -0.7T) magnetic field and 0.01–1 mA of current were used during the Hall measurement, which was performed at room temperature.

Sputter deposition of NiO_x and Pt:

n-InP and p^+n-InP samples were cleaned by immersion for 30 s in 0.04% (v/v) Br_2/CH_3OH. The InP samples were then rinsed thoroughly with CH_3OH and were stored in CH_3OH before being dried with N_2(g) and loaded into the sputtering chamber. Reactive RF sputtering using a high-vacuum magnetron-sputtering system (AJA International Inc.) was conducted in a chamber with a maximum base pressure of 8×10^{-8} Torr and NiO_x was deposited directly onto the cleaned n-InP and n^+-InP samples and onto the p^+-emitter side of the p^+n-InP sample. The O_2 concentration ($O_2/(Ar+O_2)$) was 4.8% with a constant Ar flow of 20 sccm, and the working pressure was 5 mTorr. The substrates were maintained at 300 °C. The deposition rate was maintained at 0.2 Å s^{-1} by tuning the sputtering power on the Ni target (Kurt Lesker, 2" diameter × 0.125" thickness, 99.95%) unless otherwise specified. Thin Ni metal films were deposited under the same condition without introduction of O_2 gas. An ultrathin layer of Pt (~2 nm) was sputtered on as-

cleaned-p^+n-InP substrates using RF sputtering in the same magnetron sputtering system at 300 °C.

Characterization and properties of NiO_x:

Sputter-deposited NiO_x films produced using different deposition conditions were characterized using x-ray diffraction (XRD), scanning-electron microscopy (SEM), atomic-force microscopy (AFM), x-ray photoelectron spectroscopy (XPS), UV-vis spectroscopy, spectroscopic ellipsometry, Mott-Schottky (M-S) measurements, and transmission-electron microscopy (TEM). Detailed characterization can be found eleswhere [1]. Briefly, the oxygen concentration during the reactive sputtering process produced films with different conductivity and catalytic activity. Films prepared using oxygen concentration ≤ 4.8% produced material with comparable catalytic activity and electrical conductivity across its thickness. XPS revealed a mixture Ni(II) and Ni(III) at the surface, and the ratio was affected by the O_2 concentration during deposition. Moreover, the oxygen concentration and the substrate heating temperature affected the crystalline structure and the optical properties, as well as the catalytic performance, of the resulting films. SEM, AFM and TEM studies revealed a columnar structure in the prepared film with a grain size that was controlled by the deposition conditions, including the O_2 concentration, deposition rate and substrate heating temperature. Spectroscopic ellipsometry revealed an anisotropy in the refractive indices as well as electrical conductivity along different directions and at different positions along the film, which originated from the structural properties of the prepared films. UV-vis spectroscopy and ellipsometry both revealed a direct optical band gap of 3.74 eV and negligible absorption in the visible range on films prepared with proper substrate heating. Mott-Schottky measurements in contact with an electrochemically reversible one-electron redox-couple revealed that the films were p-type with a doping level of ~10^{19} cm^{-3}.

Electrode preparation:

Ohmic contacts were formed by scribing an In-Ga eutectic alloy (Alfa Aesar, 99.99%) onto the back (n-doped) side of the n-InP and p^+n-InP samples. To form an ohmic contact to p^+-InP, a sequential evaporation of 100 Å Au, 1000 Å Zn, and 700 Å Au followed by annealing at 500 °C for 15 min under forming gas was used to form an ohmic contact[2]. High-purity Ag paint (SPI supplies) was used to mechanically attach the ohmic contact to a coiled, tin-plated Cu wire (McMaster-Carr) which was then threaded through a glass tube (Corning Incorporation, Pyrex tubing, 7740 glass). The sample was encapsulated and sealed to the glass tube using a mixture of 2:1 grey epoxy (Hysol 9460F) and white epoxy (Hysol 1C). The epoxy was allowed to dry under ambient conditions for > 12 h. A high-resolution optical scanner (Epson perfection V370 with a resolution of 2400 psi) was used to image the exposed surface area of each electrode, and the geometric areas were determined by analyzing the images using ImageJ software. All of the electrodes in this study were 0.06-0.12 cm^2 in area unless otherwise specified.

Electrochemical measurement:

A Mercury/Mercury oxide (Hg/HgO in 1.0 M KOH(aq), CH Instruments, CH152) electrode was used as the reference electrode, and a carbon cloth placed within a fritted glass tube (gas dispersion tube Pro-D, Aceglass, Inc.) was used as the counter electrode for all electrochemical measurements performed in 1.0 M KOH(aq), including photoelectrochemical, spectral response, in situ transmission measurement, and Faradaic efficiency measurements. The Hg/HgO reference electrode was calibrated versus the reversible hydrogen electrode (RHE), and the Hg/HgO electrode potential was determined to be 0.926 V versus RHE. The equilibrium potential for the oxygen-evolution reaction was therefore 0.304 V versus the Hg/HgO reference. 1.0 M boric acid buffered KOH (K-Bi) aqueous solution was made of 2.0 M boric acid and 1.0 M KOH. For measurement in 1.0 M K-Bi(aq), a saturated calomel electrode (SCE, saturated KCl, CH

Instruments, CH150) was used as the reference electrode, and a fritted Pt mesh was used as a counter electrode. The SCE electrode was calibrated versus the RHE electrode and the SCE potential was determined to be 0.813 vs. RHE. The equilibrium potential for water oxidation was therefore 0.417 V vs. SCE in 1.0 M K-Bi(aq).

A custom electrochemical cell with a flat glass (Pyrex) bottom was used for all of the electrochemical measurements. During measurements, the electrolyte was vigorously agitated with a magnetic stir bar driven by a model-train motor (Pittman) with a Railpower 1370 speed controller (Model Rectifier Corporation). The data presented for electrochemical measurements in aqueous solutions do not include compensation for the series resistance of the solution. ELH-type (Sylvania/Osram) and ENH-type (EIKO) tungsten-halogen lamps with a dichroic rear reflector and a custom housing with a transformer (Staco Energy Products Co.) were used for photoelectrochemical stability measurements. A Xe arc lamp (Newport 67005 and 69911) equipped with an IR filter (Newport 61945) and with an AM 1.5 filter (Newport 81094 and 71260) was used as the light source for *J-E* measurements and for the spectral response measurements. The illumination intensity at the position of the working electrode in the electrochemical cell was determined by placing a calibrated Si photodiode (FDS100-Cal, Thor Labs) into the cell at the same position occupied by the exposed area of the photoelectrode. To illuminate bottom-facing photoelectrodes, a quartz diffuser (Newport 15Diff-Vis) together with a broadband reflection mirror (Newport dielectric mirror, 10Q20PR-HR) was used to direct the uniform light beam from the horizontal to the vertical direction.

Cyclic voltammetry as well as quantum yield data were obtained using a Biologic SP-200 potentiostat, whereas stability data were obtained using a MPG-2 multichannel potentiostat (Bio-Logic Science Instruments). The cyclic voltammetric data were recorded at a scan rate of 40 mV s^{-1} unless specified, with a scan range that varied depending on the photovoltage of the sample.

The external quantum yield was determined by connecting the potentiostat to a lock-in amplifier, with the light chopped at 20 Hz.

Faradaic efficiency measurement at low current density:

A Neofox fluorescence probe (Foxy probe, Ocean Optics) was used to monitor the concentration of O_2 throughout the experiment. The fluorescence response was calibrated against the standard concentration of oxygen in water (7700 μg L^{-1} or 2.4×10^{-4} M) under a standard atmosphere that contained 20.9% (by volume) O_2(g). The fluorescence probe, the Hg/HgO/1.0 M KOH reference electrode, a fritted Pt mesh counter electrode (Alfa-Aesar, 100 mesh, 99.9% trace metal basis), and the NiO_x-coated semiconductor working electrodes with geometric surface areas of 0.284-0.481 cm^2 were loaded into an airtight glass cell that had a volume of 43.6 mL with no headspace, and that was equipped with four ports and a side-facing quartz window. The cell and the 1.0 M KOH(aq) electrolyte in the cell were purged with a stream of ultra-high purity Ar(g) for ~1 h prior to the measurement of the O_2 produced. The electrode was maintained in the water bath to minimize temperature fluctuations during illumination. The current density was maintained at 1 mA cm^{-2} or lower, to prevent bubble formation on the electrode surfaces. The fluorescence probe was in the dark during the measurement. To compare the charge versus time data from the potentiostat with the amount of oxygen generated versus time for a system operating at 100% Faradaic efficiency, the charge passed (in mA·h) was multiplied by 3.6 to convert the data into coulombs, and the result was then multiplied by 83 (the factor for conversion of 1 C of electrons to 1 μg of O_2) to convert the value into micrograms of O_2.

Faradaic efficiency measurement:

Measurements of Faradaic efficiency based on collection of the evolved gas were conducted using a custom experimental set-up consisting of an inverted burette connected to a three-necked electrochemical cell using the two-compartment electrochemical setup configured as described above. The 1.0 M KOH(aq) was first saturated with hydrated high-purity O_2(g) for 2 h prior to the measurement. Electrodes with surface areas of 0.5-0.7 cm^{-2} were placed inside the inverted burette for enhanced gas collection efficiency. Samples, including Ni foil control samples and NiO_x coated n^+-InP dark electrodes, were first activated by potential cycling in 1.0 M KOH(aq). A constant current of 5 mA was then applied and maintained on the samples throughout the measurement. The expected volume of generated O_2 (ml) was calculated based on the charge passed (C in coulombs) using the equation:

$$O_2\ volume(ml) = \frac{1000 \cdot T \cdot \rho \cdot C}{4 \cdot F \cdot M_w} \quad \text{(S1)}$$

where T is temperature (296.45 K), ρ is the O_2 density at atmospheric pressure (1.43 g cm^{-3}), C is the total charge passed (C), F is Faraday's constant (9.65×10^4 C mol^{-1}), and M_w is the molar weight of O_2 (15.99 g mol^{-1}). The Faradaic efficiency was calculated as the ratio of the measured to the expected O_2 volume.

Photocurrent density from integration against the AM 1.5G spectrum:

The integrated photocurrent density according to the measured external quantum yield under the spectral distribution of the standard AM 1.5G spectrum was calculated using the following equation:

$$J = \int_{\lambda=350}^{\lambda} {}^{q}/_{hc}\, \Phi_{\text{ext}}(\lambda) \cdot E(\lambda) \cdot \lambda \cdot d\lambda \approx \int_{\lambda=350}^{\lambda} {}^{\Phi_{\text{ext}}(\lambda) \cdot \lambda}/_{1240} \cdot E(\lambda) \cdot d\lambda \quad \text{(S2)}$$

where J is the integrated photocurrent density in A m^{-2}, h is Planck's constant (6.63×10^{-34} J s), and c is the speed of light (2.998×10^8 m s^{-1}), q is elementary charge (1.602×10^{-19} C), Φ_{ext} is the

measured external quantum yield, E is the irradiance in W m^{-2} nm^{-1}, λ is the light wavelength in nm, 1240 is in W nm A^{-1}, and $\Phi_{ext} \cdot \lambda/1240$ is the responsivity in A W^{-1}.

Calculation of total reflectance and thickness design of antireflective NiO_x coating on InP:

Total reflectance spectra of InP|NiO_x samples with different NiO_x thickness (varied from 0-320 nm) with air or water as incident media were obtained based on calculation of the propagation matrix of plane waves at dielectric interfaces. Matlab functions (*multidiel*), by Sophocles J. Orfanidis from Rutgers University, were used to calculate the reflection responses of isotropic non-lossy isotropic multilayer-dielectric structures. The optical constants of water and InP were adopted from reported values[3]. The refractive index of the sputtered NiO_x films was measured using spectroscopic ellipsometry with an autoretarder. Maximum photocurrent densities at different NiO_x thickness with either air or water as incident media were calculated based on the reflection spectra and the AM 1.5G solar spectrum, assuming unity quantum efficiency from the InP substrate considering the optical absorption of a water layer. The total percentages of reflected light were calculated based on the ratio between the integrated power of the reflected spectrum and the incident AM 1.5 solar spectrum. The absorption coefficient of water was also considered using reported values in the study of water layer thickness effect on the maximum photocurrent density.

Calculation of charge needed to dissolve the InP wafer:

The total charge needed to dissolve the entire InP wafer was calculated using:

$$C = 6 \cdot \frac{\rho t}{M_w} F \quad \text{(S3)}$$

where C is the total charge needed to dissolve the entire InP wafer in C cm^{-2}, ρ is the density in g cm^{-3}, t is the thickness in cm, and M_w is the molar weight in g mol^{-1} of InP, and F is the Faraday's constant (9.6485×10^4 C mol^{-1}).

Ohmic contact between NiO_x and InP substrate:

NiO_x coated n-InP and n^+-InP showed ohmic behavior, due to the surface Fermi-level pinning, and thus exhibited a low barrier height for charge separation. However, addition of a p^+-InP homogeneous junction formed a buried junction and isolated the shunting pathways by forming a diode that blocked majority carriers from flowing across the interface in the dark, therefore no dark catalysis current but only a small reverse leakage current was observed for such structures. Without formation of alloyed metal contacts to the p^+-InP emitter, the direct NiO_x coated np^+-InP led to lower photovoltages and poor fill factors. Therefore, in the load-line analysis n^+-InP|NiO_x was used as the dark reference instead of p^+-InP substrates. To improve the junction properties, a thin layer of Pt was used to improve the junction between the p^+-InP emitter and NiO_x by providing a high work function metal that could also partially prevent InP oxidation during NiO_x deposition. AFM images of 2-nm Pt did not show a continuous film. Although an improved contact resistance was observed, introduction of Pt increased the dark current due to the increased shunting pathways.

Supporting figures:

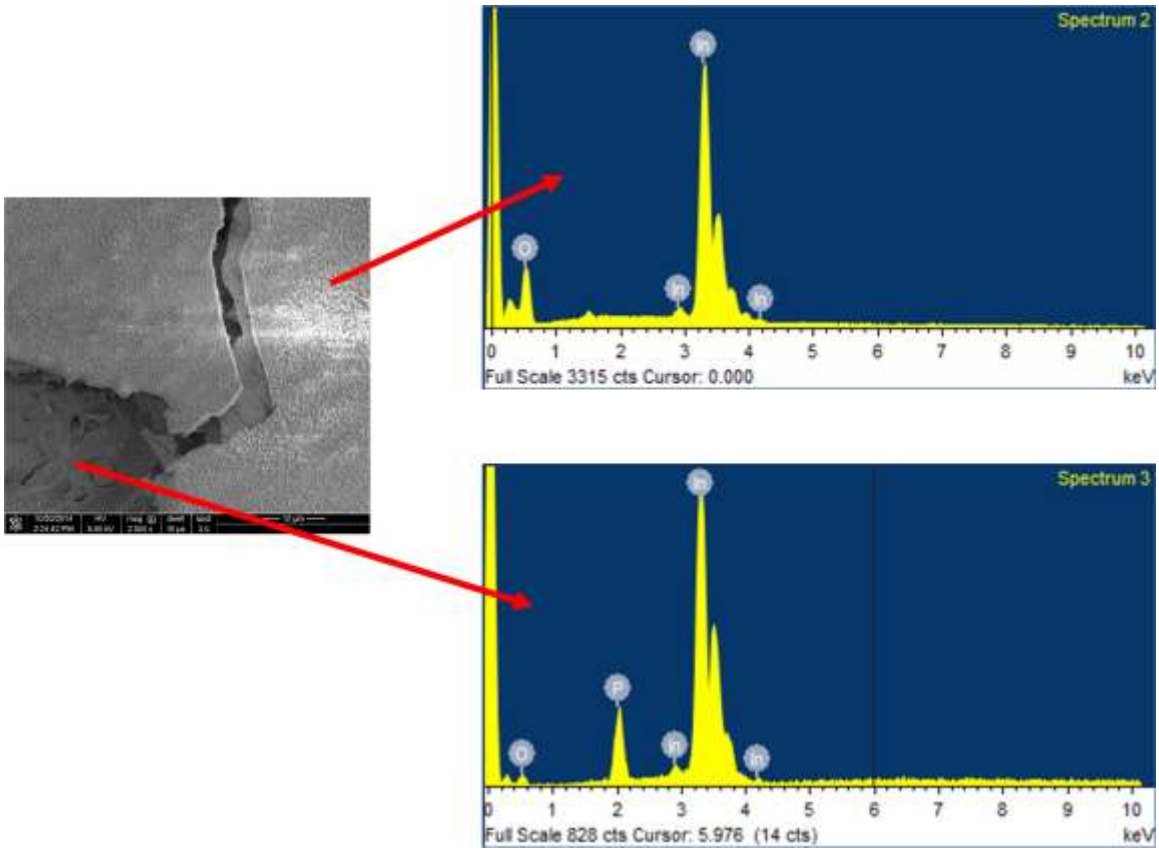

Figure s1. SEM image of a bare n^+-InP dark electrode without NiO_x after operation in 1.0 M KOH (aq) after the passage of 48 C cm^{-2} of charge density, showing a damaged surface. The EDX spectra showed the formation of a thick In_2O_3 layer (on the top) and bulk InP remained at the bottom (at the bottom).

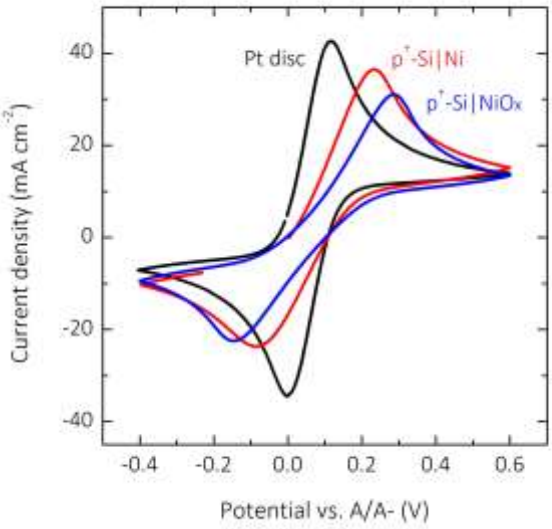

Figure s2. *J-E* behavior of metallic Ni and NiO_x-coated p^+-Si electrodes in contact with $Fe(CN)_6^{3-/4-}$ (aq) with 1.0 M KCl as supporting electrolyte. The behavior of a Pt disc electrode is shown for comparison.

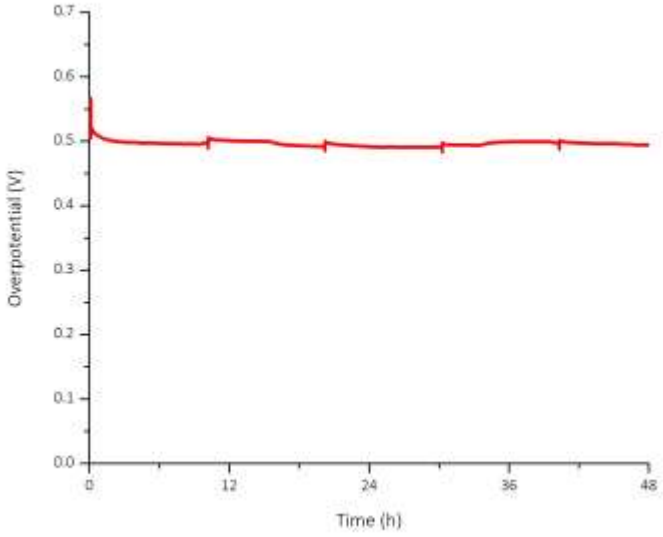

Figure s3. Chronopoteniometric stability of an n-InP|NiO_x dark electrode operated at 20 mA cm^{-2}.

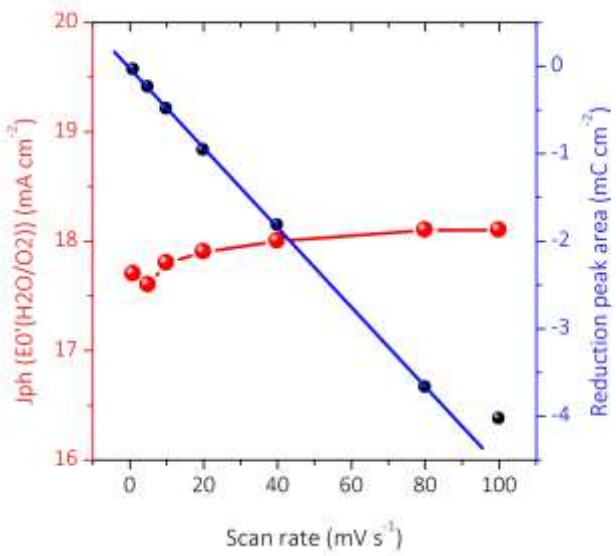

Figure s4. Photocurrent density at the equilibrium potential for water oxidation and area of the reduction peak in the Ni redox peaks as a function of scan rate. The measured *J-E* data were not a function of the scan rate, with the variation of the current density at the equilibrium oxygen evolution potential vs. scan rate falling within the error bar of the experiment, as measured on 3 independent samples. The scan rate did affect the cathodic current density described by the Ni redox peaks, which showed a linear relationship between the peak current and the scan rate over most of the range of scan rates studied.

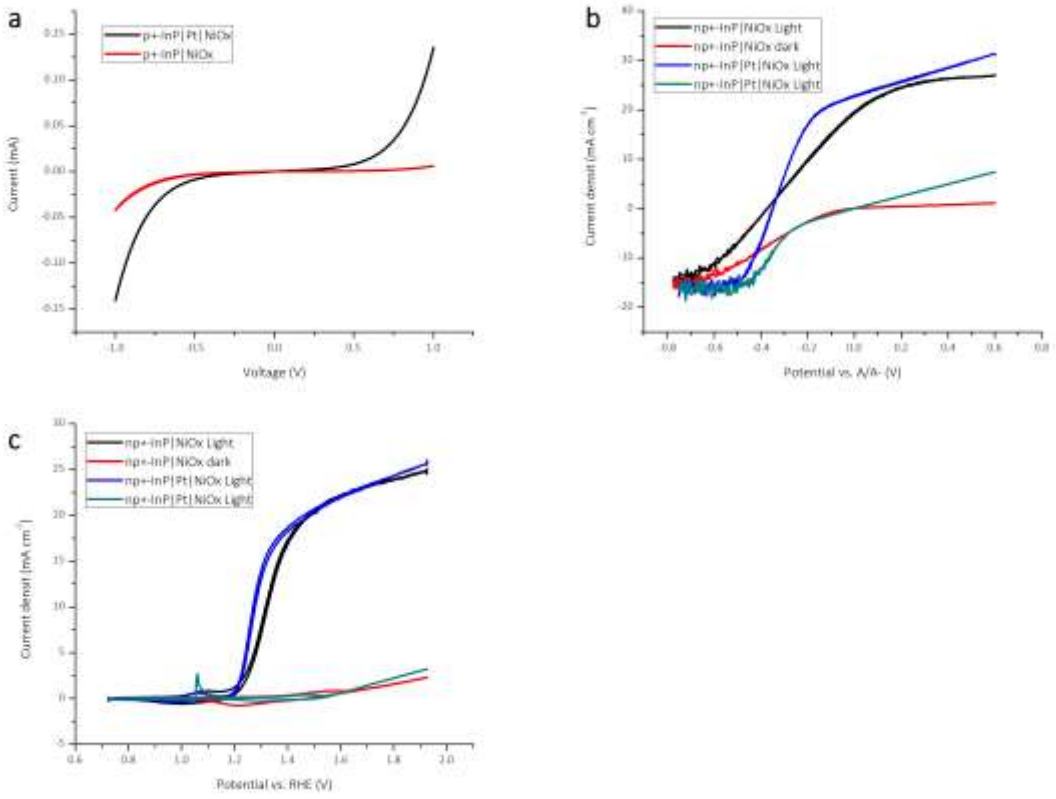

Figure s5. (a) Solid-state device measurements and electrochemical measurements in (b) $Fe(CN)_6^{3-/4-}$ (aq) with 1.0 M KCl as supporting electrolyte and (c) 1.0 M KOH (aq) showing the reduced series resistance and enhanced shunting resistance through the intermediate Pt layer between the p^+-InP emitter and the functional NiO_x catalyst.

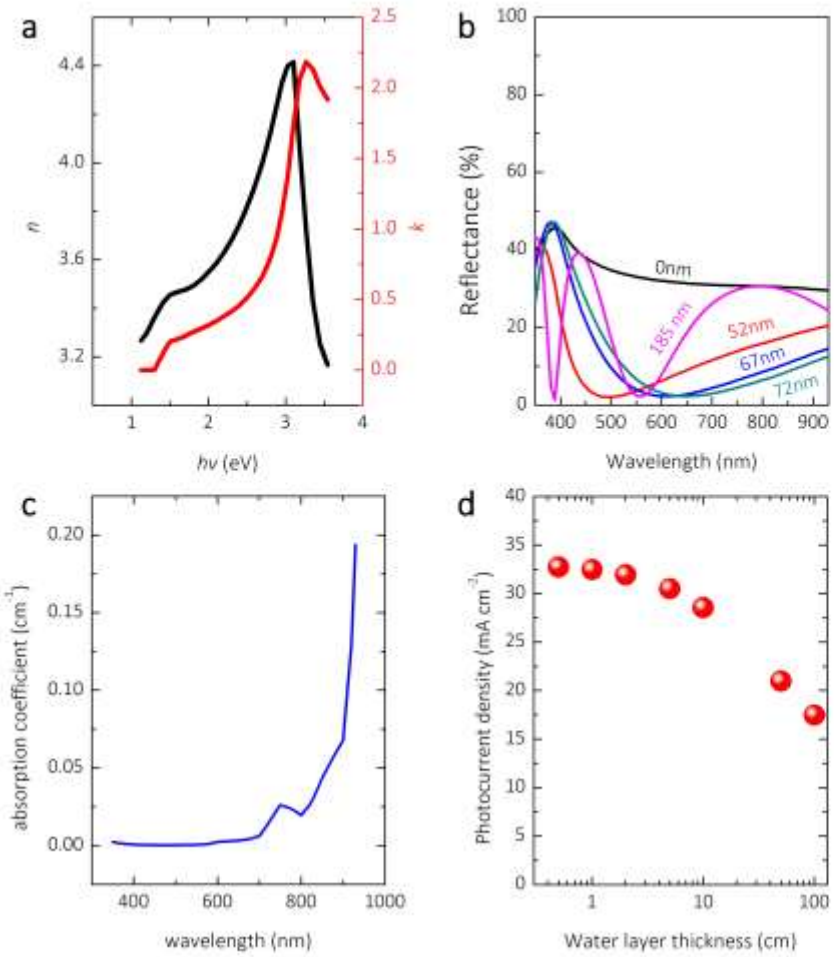

Figure s6. (a) Optical constants of crystalline InP. (b) Calculated reflectance spectra of InP homogeneously coated with NiO_x of different thicknesses in air as the incident medium, based on a non-lossy NiO_x layer; (c) Absorption coefficient of water; and (d) maximum photocurrent density of InP coated with 70 nm of NiO_x as a function of the thickness of the water layer.

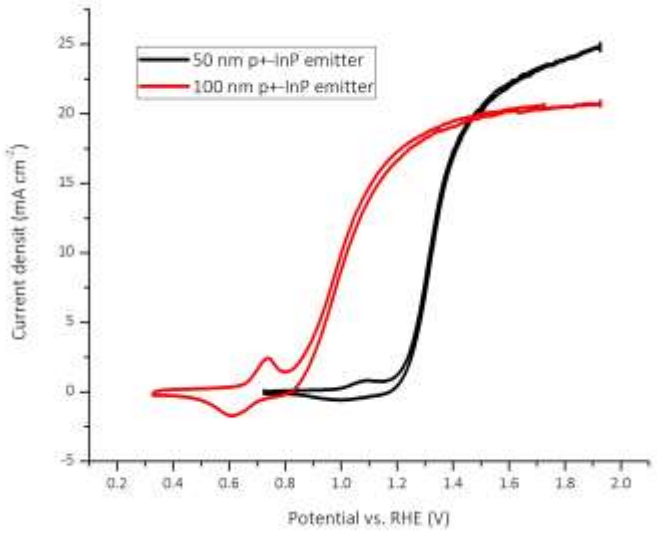

Figure s7. *J-E* behavior of a NiO_x coated p^+n-InP photovoltaic cell as a function of the emitter thicknesses (red curve: 100 nm and black curve: 50 nm).

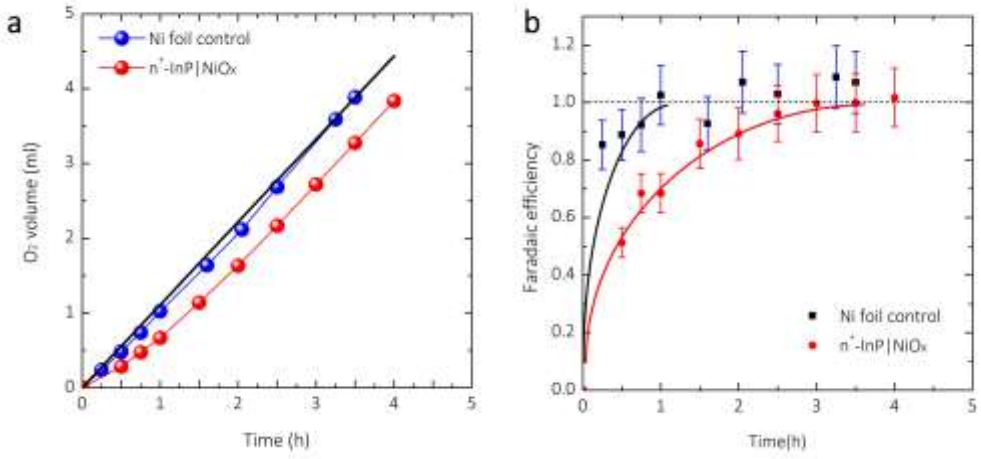

Figure s8. (a) Volume of collected O_2 vs. time on a conditioned Ni foil electrode (blue) and an n^+-InP|NiO_x electrode (red) at a constant current of 5 mA. The black line shows the volume of the expected O_2 calculated based on the total charge passed; and (b) Faradaic efficiency calculated

based on the volume ratio of the measured O_2 and the expected O_2. Black and red solid lines are used to guide the eye. 10% systematic measurement error from volume reading were added.

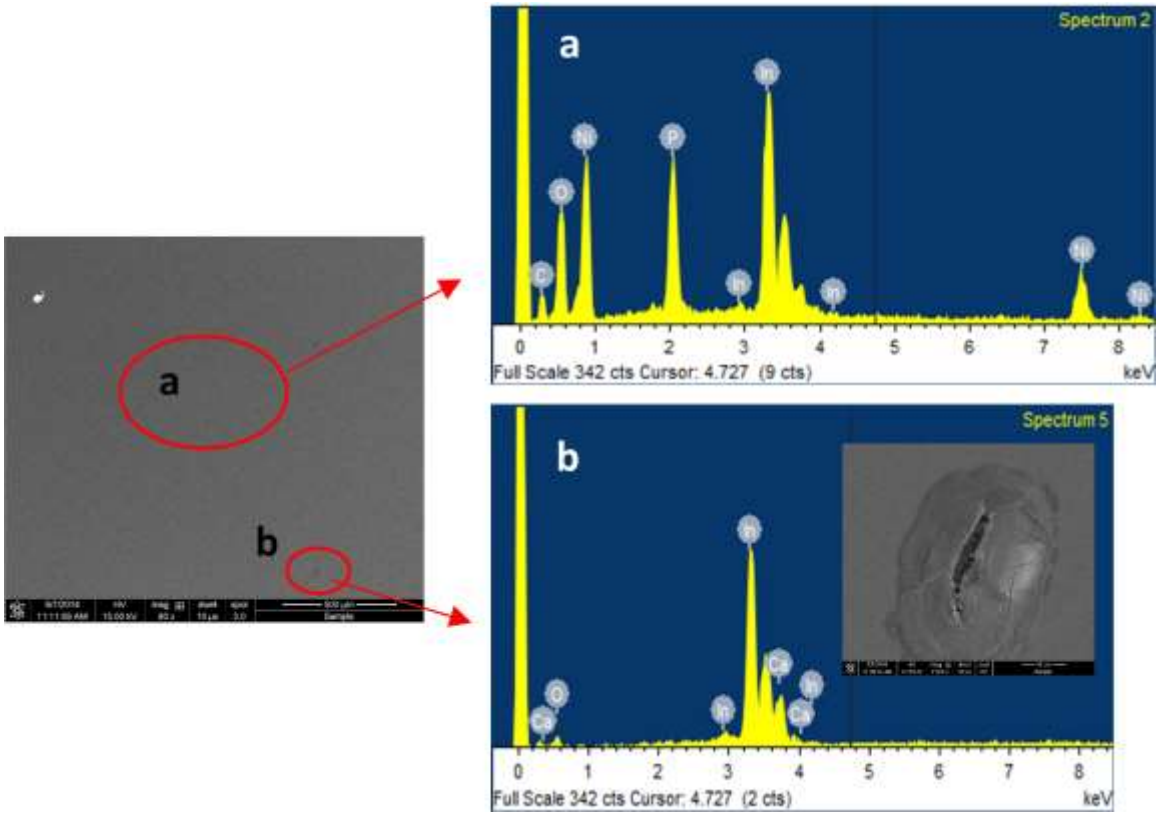

Figure s9. SEM image of an n^+-InP|NiO_x electrode after operation in 1.0 M KOH(aq) at 20 mA cm^{-2} for 100 h, showing minor physical defects on the film surface. EDX spectra at the defects (b) and the rest of the area (a) showing the formation of an In_2O_3 passivation region.

References:

[1] K. Sun, M. T. McDowell, A. C. Nielander, S. Hu, M. R. Shaner, F. Yang, B. S. Brunschwig, N. S. Lewis, J. Phys. Chem. Lett. 2015, 6, 592; K. Sun, F. H. Saadi, M. F. Lichterman, W. Hale, H.-p. Wang, X. Zhou, N. Plymale, S. Omelchenko, J.-H. He, B. S. Brunschwig, N. S. Lewis, Private communication 2015; X. Zhou, R. Liu, K. Sun, D. Friedrich, M.

T. Mcdowell, F. Yang, S. Omelchenko, F. H. Saadi, A. C. Nielander, B. S. Brunschwig, N. S. Lewis, Private communication 2015.

[2] K. E. Pomykal, A. M. Fajardo, N. S. Lewis, J. Phys. Chem. 1996, 100, 3652.

[3] D. E. Aspnes, A. A. Studna, Phys. Rev. B: Condens. Matter 1983, 27, 985; G. M. Hale, M. R. Querry, Appl. Opt. 1973, 12, 555.